Nested Hash Layer: A Plug-and-play Module for Multiple-length Hash Code Learning

Liyang He¹, Yuren Zhang¹, Rui Li¹, Zhenya Huang¹, Runze Wu², Enhong Chen¹

¹State Key Laboratory of Cognitive Intelligence, University of Science and Technology of China; ² NetEase Fuxi AI Lab

{heliyang,yurenz,ruili2000}@mail.ustc.edu.cn {huangzhy,cheneh}@ustc.edu.cn,wurunze1@corp.netease.com

Abstract

Deep supervised hashing is essential for efficient storage and search in large-scale image retrieval. Traditional deep supervised hashing models generate single-length hash codes, but this creates a trade-off between efficiency and effectiveness for different code lengths. To find the optimal length for a task, multiple models must be trained, increasing time and computation. Furthermore, relationships between hash codes of different lengths are often ignored. To address these issues, we propose the Nested Hash Layer (NHL), a plug-and-play module for deep supervised hashing models. NHL generates hash codes of multiple lengths simultaneously in a nested structure. To resolve optimization conflicts from multiple learning objectives, we introduce a dominance-aware dynamic weighting strategy to adjust gradients. Additionally, we propose a long-short cascade self-distillation method, where long hash codes guide the learning of shorter ones, improving overall code quality. Experiments indicate that the NHL achieves an overall training speed improvement of approximately 5 to 8 times across various deep supervised hashing models and enhances the average performance of these models by about 3.4%.

1 Introduction

With the growing amount of visual data on the Internet, existing databases are becoming vast. To manage this data in large-scale image databases, hashing represents images as binary hash codes for efficient storage and search [29]. Recently, deep supervised hashing has made significant progress by extracting deep features and using supervised signals to enhance hash code quality. As shown in the upper part of Figure 1a, the traditional approach involves using a deep neural network to extract features and a hash layer to generate hash codes¹. The hash layer typically consists of a single-layer perceptron that maps features to the desired hash code length, followed by a binary operation (e.g., the signum function) to produce the final hash codes.

However, most deep supervised hashing models focus on generating hash codes of a specific length. This leads to two problems. First, Figure 1b shows the performance of four deep supervised hashing models [27, 40, 3, 38] on the CIFAR-10 dataset at different code lengths. There is a clear trade-off between efficiency and effectiveness: shorter hash codes improve efficiency but reduce effectiveness, while longer hash codes enhance performance but increase storage and computational costs [37]. Furthermore, this trade-off is not entirely inversely proportional, as seen with the DSH model, which suffers a notable performance drop at 128 bits, a phenomenon known as the dimension curve of hash code. As a result, multiple models must be trained for different code lengths to find the best fit for a

¹Most deep hashing methods for image retrieval adhere to this paradigm, while some works [36, 16, 4, 41] optimize the hash code in the database independently. Our work focuses on the former.

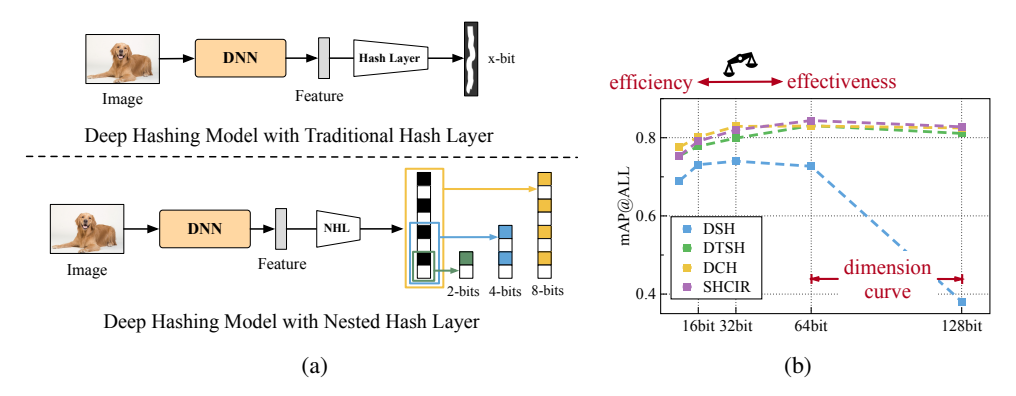


Figure 1: (a) A schematic comparison between traditional hash layer methods and our proposed NHL. The NHL can generate hash codes of multiple lengths simultaneously in a nested manner. (b) The performance of four deep supervised hashing models on the CIFAR-10 dataset highlights the uncertainty in effectiveness and efficiency under different code lengths.

specific task, greatly increasing training time and resource use [42]. Second, since these models only produce single-length hash codes, they overlook the potential relationships between hash codes of different lengths. This raises a question: is it possible to train a single hashing model capable of producing hash codes of multiple lengths?

Code expansion and compression-oriented deep hashing methods address the variation in hash code lengths after training. They generate new codes either through code expansion [31, 42, 43] or compression [46]. However, their primary focus is on learning a mapping after model training to convert existing hash codes into new ones. MAH [30] and SDMLH [32] involve the generation of hash codes with multiple lengths, but they rely on specifically designed models that cannot be generalized to other deep hashing models. Thus, designing a method capable of being widely applied to deep hashing models for generating hash codes of multiple lengths remains an unexplored area.

In this work, we propose the Nested Hash Layer (NHL), a plug-and-play module that replaces the traditional hash layer in deep supervised hashing models to generate hash codes of multiple lengths. **First**, we observe that deep supervised hashing models use the same backbone to extract features, regardless of code length. Additionally, longer hash codes can be seen as extensions of shorter ones. Based on these insights, the NHL is designed as shown in the lower part of Figure 1a to generate hash codes of different lengths in a nested manner, enabling multiple-length code generation in one model. **Second**, while the NHL combines objectives for multiple code lengths, conflicts may arise, as shorter hash codes are integral to longer ones. Thus, we introduce a Dominance-Aware Dynamic Weighting strategy. We define a "domination gradient" for each nested parameter, prioritizing the optimization of shorter hash codes. By monitoring parameter gradients, we dynamically adjust objective weights to align with the domination gradient and avoid conflicts. **Third**, unlike the traditional hash layer, NHL generates multiple-length hash codes. To further enhance code quality, we propose a Long-short Cascade Self-distillation method, leveraging the relationships in long hash codes to guide and improve shorter ones.

As evidenced by extensive experiments and analysis, NHL offers the following key advantages: (1) NHL achieves an overall training speed improvement of approximately 5 to 8 times across various deep supervised hashing models. (2) While ensuring faster training, NHL enhances the average performance of these models by about 3.4% and remarkably alleviates the dimensionality curse of hash codes. (3) NHL demonstrates exceptional flexibility in adapting to scenarios with multiple hash code length settings and different backbones.

2 Related work

2.1 Deep Supervised Hashing

Our work focuses on deep supervised hashing models, which can be roughly divided into pair-wise methods, ranking-based methods, and proxy-based methods. The objective of pair-wise methods

[27, 48, 49, 3, 23, 47] is to ensure similar pairs have similar hash codes while dissimilar pairs have dissimilar hash codes. Ranking-based methods adopt ranking-based similarity-preserving loss terms. For instance, triplet loss [40, 25] and list-wise loss [2] are commonly used to maintain data ordering. Proxy-based methods [45, 9, 14, 38, 39], also known as center-based methods, have emerged as a widely acclaimed approach recently. These methods first generate each category's proxies (or hash centers). Then, they force hash codes outputted from the network to approach corresponding proxies (or hash centers). Most of the current deep supervised hashing models only account for a single model with a specific code length. This limitation leads to slow training in practical applications due to the need to train multiple models with different hash code lengths. MAH [30] and SDMLH [32] attempt to solve this problem, but they rely on specifically designed models that cannot be generalized to other deep hashing models.

2.2 Multi-task Learning

The NHL can be seen as a multi-task learning framework [22], where multiple related tasks are trained simultaneously using a shared model. Its primary function is to enable a single hash model to serve multiple learning objectives for different code lengths. A key aspect of multi-task learning is architecture design, including hard parameter sharing methods [19, 1] and soft parameter sharing methods [34, 10, 28]. NHL only makes simple adjustments to the hash layer to accommodate various deep hashing models. MRL [21] partly inspired its basic structure, which generates representations of different lengths for multiple tasks. However, MRL does not address gradient conflicts or the relationships between representations of different lengths.

To address gradient or task conflicts, some methods re-weight the task losses based on specific criteria such as uncertainty [17], gradient norm [5], or difficulty [12]. Other methods leverage gradient information to modify the gradient on the parameter update procedure [44, 6, 26, 15]. Nevertheless, these multi-task learning methods assume the importance of different objectives is equivalent. In NHL, the weights of objectives are different because the short hash codes appear to hold greater significance. Resolving this problem remains a further exploration.

3 METHODOLOGY

3.1 Problem Definition

Given a database $X=\{x_i\}_{i=1}^N$ comprising N images and $Y=\{y_i\}_{i=1}^N$ is the corresponding label set, deep supervised hashing targets to learn a hash function $f:x_i\mapsto h_i$ that maps each data $x_i\in X$ to a binary hash code $h_i\in\{-1,1\}^b$, where b denotes the length of hash code. This mapping aims to preserve the pairwise similarities between the images x_i and x_j in the Hamming space, characterized by the Hamming distance for hash codes h_i and h_j . In this work, we aim to generate hash codes with m code lengths $b=\{b_k\}_{k=1}^m$. Without loss of generality, we define $b_k < b_{k+1}$. Then, the image x_i is mapped to m different lengths of hash codes, denoted as $\{h_i^{(k)}\}_{k=1}^m$.

3.2 Hash Code Generation

The process of acquiring hash codes of most deep supervised hashing methods is divided into two parts. First, a deep neural network is employed to extract the feature $v = \mathcal{F}(x) \in \mathbb{R}^l$ given the data $x_i \in X$, where l is the dimension of v. Then, a hash layer is utilized to derive the hash code h. In most cases, the hash layer consists of a single-layer perceptron to map the data features to a length equivalent to that of the hash code, and an operation ϕ for acquiring the hash codes. The whole process to get the hash code h can be formulated as follows:

$$h = f(x) = \phi(WF(x) + c), \tag{1}$$

where $\mathcal{W} \in R^{b \times l}$ and $c \in R^b$ are the parameters in the single-layer perception to be learned. Current deep hashing methods usually predefine a code length b_k and then train a hash model f_k accordingly. However, in practice, the selection of an appropriate code length depends on the specific task at hand, which means we need to train multiple deep hashing models $\{f_k\}_{k=1}^m$ for different code lengths and select the most suitable one. Such an approach will increase both the training time and computational resources required. To solve this problem, we introduce NHL to replace the original hash layer in deep hashing models. In the following section, we omit the bias c and the operation ϕ for conciseness.

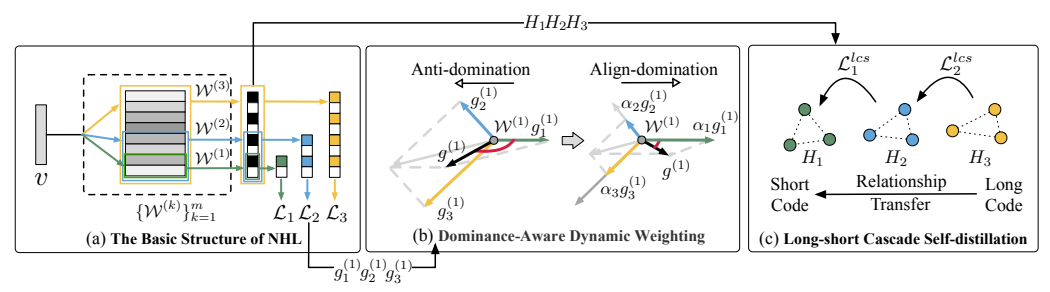


Figure 2: (a): The Nested Hash Layer (NHL) can generate m (here, m=3) hash codes with varying lengths in one training procedure. (b) The illustration of the Dominance-Aware Dynamic Weighting strategy. Taking the $\mathcal{W}^{(1)}$ as an example. (c) The Long-short Cascade Self-distillation transfer relationship from long hash codes to short hash codes.

3.3 Basic Structure of Nested Hash Layer

Although the predefined code lengths differ, the same backbone is employed for a specific deep hashing model. Inspired by this observation, we propose the basic structure of NHL to help deep hashing models generate hash codes with different code lengths in one training procedure.

As shown in Figure 2a, NHL uses a nested parameter $\{\mathcal{W}^{(k)}\}_{k=1}^m$ to achieve this goal without adding additional parameters to the neural network. The parameter $\mathcal{W}^{(k)} = \mathcal{W}^{(m)}_{[1:b_k]} \in \mathbb{R}^{l \times b_k}$ is in a nested structure, which means $\mathcal{W}^{(k)} \subset \mathcal{W}^{(k+1)}$. It uses the first b_k vectors of the parameter $\mathcal{W}^{(m)} \in \mathbb{R}^{l \times b_m}$. We can obtain the hash codes with different lengths $\{h^{(k)}\}_{k=1}^m$ through $h^{(k)} = \phi(\mathcal{W}^{(k)}v^T)$. Then, we aim to minimize the following objective.

$$\mathcal{L} = \sum_{i=1}^{N} \sum_{k=1}^{m} \mathcal{L}_k(h_i^{(k)}, y_i; \theta_F, \mathcal{W}^{(k)}),$$
 (2)

where θ_F is the parameter of backbone, and \mathcal{L}_k is the objective of a specific deep hashing model for code length b_k . In most deep hashing models, \mathcal{L}_k can be a combination of multiple objectives, such as the central similarity loss and quantization loss. As it simply involves adding the original objective of the deep hashing model, it does not alter the original optimization method. By minimizing Eq.(2), we force hash codes with different lengths to ensure their performance.

3.4 Dominance-Aware Dynamic Weighting strategy

Although basic NHL can generate hash codes with different lengths, we are unable to predict whether the gradients for different objectives $\{\mathcal{L}_k\}_{k=1}^m$ are mutually beneficial or detrimental. For example, in the left part of Figure 2b, the parameter $\mathcal{W}^{(1)}$ is updated by three gradients $g_1^{(1)} = \frac{\partial \mathcal{L}_1}{\partial \mathcal{W}^{(1)}}$, $g_2^{(1)} = \frac{\partial \mathcal{L}_2}{\partial \mathcal{W}^{(1)}}$, and $g_3^{(1)} = \frac{\partial \mathcal{L}_3}{\partial \mathcal{W}^{(1)}}$. Due to the impact of $g_2^{(1)}$, $g_3^{(1)}$, optimizing the parameters tends to proceed in a direction unfavourable to $g_1^{(1)}$ because the negative inner product between $g_1^{(1)}$ and $g_2^{(1)}$, $g_3^{(1)}$. However, The quality of the hash code $h^{(1)}$ is determined by objective \mathcal{L}_1 , which updates $\mathcal{W}^{(1)}$ using the gradient $g_1^{(1)}$ based on the target's outcomes. Therefore, if the final optimization direction of $\mathcal{W}^{(1)}$ diverges from $g_1^{(1)}$, it is highly probable that such a deviation will lead to a deterioration in the quality of $h^{(1)}$ because the wrong optimization direction for it.

Some multi-task learning works [44, 6, 26, 15, 11] propose modifying the gradient on the parameter update procedure to prevent gradient conflicts. However, there exists a difference between these multi-task learning settings and NHL. Multi-task learning treats diverse learning objectives as equally important, aiming to balance various learning objectives. In NHL, the objectives corresponding to shorter hash codes appear to hold greater significance, as shorter hash codes are shared by a larger number of longer hash codes. To address this problem, we propose a dominance-aware dynamic weighting strategy to adjust the weight α_k of each objective \mathcal{L}_k by monitoring the gradients. Then

the objective Eq. (2) becomes follows:

$$\mathcal{L} = \sum_{i=1}^{N} \sum_{k=1}^{m} \alpha_k \mathcal{L}_k(h_i^{(k)}, y_i; \theta_F, \mathcal{W}^{(k)}).$$
 (3)

Since shorter hash codes should be given higher optimization priority, we are motivated to introduce the following definitions.

Definition 1 (Dominant gradient). Assume the gradient of \mathcal{L}_i for $\mathcal{W}^{(k)}$ is denoted as $g_i^k = \frac{\partial \mathcal{L}_i}{\partial \mathcal{W}^{(k)}}$. We define $g_k^{(k)} = \frac{\partial \mathcal{L}_k}{\partial \mathcal{W}^{(k)}}$ is the dominant gradient, and k=1,2...,m. For example, $g_1^{(1)}$ is the dominant gradient in Figure 2b.

Definition 2 (Anti-domination & Align-domination). Assume the gradient of $\mathcal L$ for $\mathcal W^{(k)}$ is $g^k = \frac{\partial \mathcal L}{\partial \mathcal W^{(k)}}$. We define anti-domination for the update of $\mathcal W^{(k)}$ if the inner product is negative between $g^{(k)}$ and the dominant gradient $g_k^{(k)}$, whereas a positive inner product is termed align-domination.

The dominant gradient $g_k^{(k)}$ serves as a guiding principle for the optimization of the parameter $\mathcal{W}^{(k)}$. Anti-domination and align-domination are thus employed to ascertain whether the update result of $\mathcal{W}^{(k)}$ is congruent with or divergent from the dominant gradient $g_k^{(k)}$. For example, the left part of Figure 2b shows that the update of $\mathcal{W}^{(1)}$ is anti-domination because the negative inner product between the gradient $g_k^{(1)}$ and $g_k^{(1)}$. We conducted an analysis to observe the occurrence of anti-domination as training progressed. Figure 3 depicts the likelihood of anti-domination occurring about parameter $\mathcal{W}^{(1)}$ at each epoch. These results reveal the probability of anti-domination steadily rises over time, eventually stabilizing at a level exceeding 90%. This trend signifies a growing prevalence of anti-domination scenarios as the training progresses.

Our goal is to avert anti-domination for each $\mathcal{W}^{(k)}$. We propose the following proposition:

Proposition 1. Assume $\theta_{ij}^{(k)}$ is the angle between two gradients $g_i^{(k)}$ and $g_j^{(k)}$, and $\|\cdot\|$ denotes the Frobenius norm, if the following inequality holds:

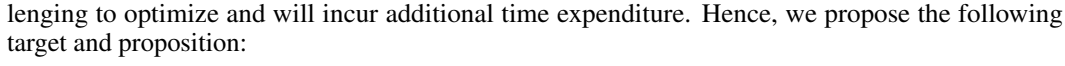
$$\alpha_k \|g_k^{(k)}\| + \sum_{k < i \leq m} \alpha_i cos\theta_{ik}^{(k)} \|g_i^{(k)}\| \geq 0,$$

then the update of $W^{(k)}$ is guaranteed to be align-domination.

be align-domination.

The proof is provided in Appendix B. How-

The proof is provided in Appendix B. However, the linear programming Eq.(4) is chal-



Proposition 2. If the following inequality holds for all $k < i \le m$, then Eq. (4) also holds.

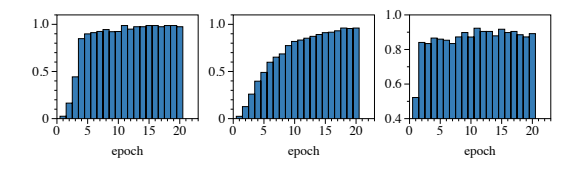
$$\alpha_i cos\theta_{ik}^{(k)} \|g_i^{(k)}\| + \frac{\alpha_k}{m-k} \|g_k^{(k)}\| \ge 0.$$
 (5)

We provide the proof in Appendix B and introduce a method to solve Eq. (5) in Appendix C. Here, for arbitrary $k \le i \le m$, we directly provide the results:

$$\alpha_i = min(\alpha_i^{(1)}, \alpha_i^{(2)}, ..., \alpha_i^{(i)}).$$
 (6)

$$\alpha_i^{(k)} = \begin{cases} 1 & \text{if } g_i^{(k)} \cdot g_k^{(k)} \ge 0\\ \frac{\alpha_k}{k - m} \frac{\|g_k^{(k)}\|^2}{g_i^{(k)} g_k^{(k)}} & \text{if } g_i^{(k)} \cdot g_k^{(k)} < 0. \end{cases}$$
(7)

In each training step, we dynamically compute the $\{\alpha_k\}_{k=1}^m$ using Eq. (6) and Eq. (7). Similar to [5], we don't consider the full network weights and focus on the parameter in NHL. The computation complex is $O(lb_mm^2)$, where l is the dimension of data feature v and b_m is the longest code length. Our experiment shows that the additional training time for each step is around 11.15%.



(a) CIFAR-10 (b) ImageNet100 (c) MSCOCO

Figure 3: The probability of anti-domination occurring on the parameter $\mathcal{W}^{(1)}$ at each epoch. We set the code lengths m=5 and use CSQ as the deep hashing models on three datasets. This trend signifies a growing prevalence of anti-domination scenarios as the training progresses.

3.5 Long-short Cascade Self-distillation

Unlike the traditional hash layer, the deep hashing model with NHL can generate hash codes of different lengths simultaneously. This leads us to explore the connections among these hash codes of different lengths. We observe a teacher-student relationship between long and short hash codes. Thus, as illustrated in Figure 2c, we propose the long-short cascade self-distillation method, which uses long hash codes to improve the performance of short hash codes in a cascading manner.

Specifically, for arbitrary image x_i , through the NHL we can get its corresponding hash codes $\{h_i^{(k)}\}_{k=1}^m$. Let $H_k = [h_1^{(k)}, h_2^{(k)}, ..., h_B^{(k)}] \in \{-1, 1\}^{B \times b_k}$ denote the matrix of hash codes with length b_k in current training batch, and B is the batch size. Then the self-distillation objectives can be formulated as:

$$\mathcal{L}_{k}^{lcs} = \frac{1}{B} \left\| \frac{h_{i}^{(k)} H_{k}^{T}}{\|h_{i}^{(k)} H_{k}^{T}\|} - \frac{h_{i}^{(k+1)} H_{(k+1)}^{T}}{\|h_{i}^{(k+1)} H_{(k+1)}^{T}\|} \right\|^{2}.$$
 (8)

Eq.(8) can be viewed as transferring the relationship between $h_i^{(k+1)}$ and other hash codes of length b_{k+1} to the relationship between $h_i^{(k)}$ and other hash codes of length b_k . Besides, we stop the gradient propagation of the long hash codes $h_i^{(k+1)}$ and $H_{(k+1)}$ to ensure that the learning of relationships is unidirectional. In other words, we only allow the shorter hash codes to learn from the relationships of the longer hash codes. By introducing the long-short cascade self-distillation into the optimization procedure, the objective Eq.(3) becomes:

$$\mathcal{L} = \sum_{i=1}^{N} \sum_{k=1}^{m-1} \alpha_k (\mathcal{L}_k + \lambda \mathcal{L}_k^{lcs}) + \sum_{i=1}^{N} \alpha_m \mathcal{L}_m, \tag{9}$$

where λ is a hyper-parameter. This method readily allows for expansion. For instance, one could explore the relationship between h_k and h_{k+a} , where a is an integer, but this is not the central concern of our work.

We renormalize the weights α_k in each step so that $\sum_{k=1}^m \alpha_k = m$ to decouple gradient re-weight from the global learning rate. Besides, in the training procedure, note that the minimum of $\mathcal L$ does not necessarily imply that each $\{\mathcal L_k\}_{k=1}^m$ is at its minimal value during the training process. Therefore, we propose a trick for our training procedure. Throughout the training, we monitor the value of each $\mathcal L_k$ and save the model parameters when each $\mathcal L_k$ reaches its minimum to output the corresponding hash codes $h^{(k)}$. We summarize the whole algorithm in Appendix D.

4 Experiments

4.1 Experiment Settings

We evaluated our method on three widely used datasets in deep hashing: CIFAR-10 [20], ImageNet100 [7], and MSCOCO [24]. We compared our approach against several state-of-the-art deep supervised hashing baselines: DSH [27], DHN [48], DTSH [40], LCDSH [49], DCH [3], DBDH [47], CSQ [45], SHCIR [38], DPN [9], and MDSH [39]. For all the above models, we adopted ResNet50 [13] as the backbone. The primary evaluation metric was mean Average Precision at top K (mAP@K). Unless otherwise specified, we set the hash code lengths $b \in \{8, 16, 32, 64, 128\}$ for the following experiments, as these lengths are prevalently used in previous works. Details regarding datasets, implementation, and evaluation settings are presented in Appendix A.

4.2 Performance on Deep Hashing Models

In this experiment, we first compared the mAP@K of different deep supervised hashing models on three datasets. Table 1 shows the results. We use "w/o NHL" to denote the deep hashing model without using NHL and use "w/ NHL" to denote the deep hashing model that uses NHL to replace the traditional hash layer. Besides, we use bold numbers to indicate statistically significant improvements when utilizing NHL compared to not using NHL, with p < 0.05 based on a two-tailed paired t-test.

We can find the following observations: (i) Globally, the implementation of the NHL leads to an average improvement of 3.398% (3.619% in CIFAR-10, 4.364% in ImageNet100, and 2.158% in

Table 1: The mAP@K comparison results on CIFAR-10, ImageNet100, and MSCOCO datasets when different deep hashing models used the original hash layer (w/o NHL) or NHL (w/ NHL). We employ bold numbers to indicate statistically significant enhancements when utilizing NHL compared to when not using NHL, with p < 0.05 based on a two-tailed paired t-test.

		l	w/o N	VHL (The	Original N	Model)		1			w/ NHL		
Data	Model	8 bits	16 bits	32 bits	64 bits	128 bits	avg.	8 bits	16 bits	32 bits	64 bits	128 bits	avg.
-	DSH	0.690	0.731	0.740	0.727	0.381	0.654	0.717	0.732	0.744	0.743	0.749	0.737 (+12.8%)
	DTSH	0.754	0.778	0.799	0.831	0.811	0.745	0.766	0.790	0.802	0.822	0.836	0.771 (+3.51%)
	DHN	0.718	0.765	0.813	0.837	0.853	0.797	0.739	0.776	0.824	0.835	0.866	0.808 (+1.38%)
	LCDSH	0.715	0.771	0.817	0.826	0.854	0.797	0.775	0.799	0.825	0.839	0.868	0.821 (+3.08%)
CIFAR-10	DCH	0.776	0.802	0.829	0.830	0.825	0.812	0.787	0.810	0.833	0.843	0.844	0.823 (+1.36%)
(mAP@ALL)	DBDH	0.737	0.771	0.796	0.829	0.829	0.792	0.748	0.785	0.804	0.825	0.844	0.801 (+1.12%)
	CSQ	0.762	0.786	0.798	0.798	0.807	0.790	0.792	0.802	0.818	0.828	0.838	0.816 (+3.21%)
	DPN	0.703	0.757	0.790	0.804	0.819	0.775	0.729	0.765	0.795	0.826	0.824	0.788 (+1.71%)
	SHCIR	0.754	0.791	0.820	0.844	0.828	0.807	0.758	0.797	0.824	0.849	0.848	0.815 (+0.99%)
	MDSH	0.755	0.808	0.829	0.844	0.832	0.814	0.762	0.811	0.838	0.852	0.861	0.825 (+1.40%)
	DSH	0.703	0.808	0.827	0.828	0.822	0.797	0.755	0.816	0.829	0.838	0.841	0.817 (+2.41%)
	DTSH	0.432	0.710	0.770	0.784	0.803	0.794	0.552	0.714	0.766	0.788	0.792	0.803 (+1.11%)
	LCDSH	0.248	0.395	0.542	0.608	0.692	0.450	0.422	0.568	0.628	0.657	0.692	0.593 (+19.4%)
ImageNet100	DCH	0.776	0.834	0.845	0.859	0.848	0.832	0.809	0.842	0.855	0.860	0.863	0.846 (+1.65%)
(mAP@1000)	CSQ	0.456	0.822	0.860	0.877	0.878	0.778	0.495	0.825	0.873	0.880	0.882	0.787 (+1.59%)
	DPN	0.436	0.827	0.864	0.870	0.877	0.775	0.487	0.829	0.860	0.877	0.881	0.787 (+1.50%)
	SHCIR	0.789	0.861	0.879	0.883	0.881	0.858	0.798	0.881	0.889	0.893	0.898	0.872 (+1.63%)
	MDSH	0.785	0.845	0.874	0.895	0.894	0.859	0.794	0.851	0.878	0.884	0.896	$0.861 \ (+0.23\%)$
	DSH	0.685	0.722	0.757	0.779	0.769	0.743	0.714	0.735	0.764	0.779	0.789	0.756 (+1.77%)
	DTSH	0.706	0.770	0.810	0.823	0.831	0.788	0.751	0.793	0.819	0.826	0.823	0.803 (+1.86%)
	DHN	0.659	0.751	0.786	0.810	0.832	0.768	0.724	0.760	0.794	0.819	0.837	0.787 (+2.47%)
MSCOCO	LCDSH	0.687	0.769	0.787	0.825	0.836	0.781	0.713	0.773	0.794	0.820	0.828	0.786 (+0.55%)
(mAP@5000)	DCH	0.695	0.756	0.762	0.777	0.734	0.745	0.723	0.769	0.786	0.788	0.789	0.771 (+3.51%)
	DBDH	0.655	0.727	0.760	0.769	0.800	0.742	0.692	0.748	0.778	0.803	0.809	0.766 (+3.23%)
	CSQ	0.596	0.750	0.847	0.877	0.871	0.788	0.659	0.778	0.847	0.878	0.881	0.809 (+2.58%)
	DPN	0.575	0.757	0.828	0.862	0.863	0.777	0.638	0.769	0.837	0.863	0.872	0.796 (+2.44%)

MSCOCO). Besides, there are 72% of cases that achieve a significant performance boost based on the two-tailed paired t-test. Conversely, only a few cases achieve a decline, with most drops of 1.37% occurring in the DTSH model when NHL is applied to the ImageNet100 dataset using a 128-bit code. Thus, we can demonstrate that NHL can yield significant improvements in the majority of cases. (ii) Deep hashing models with NHL improve significantly when the hash code length is short in some datasets. For example, in the case of 8-bit, employing NHL can increase 18.7% and 7.32% enhancement on ImageNet100 and MSCOCO datasets, respectively. (iii) It is delightful to note that NHL can address the dimensionality curse of hash code, signifying that as the code length expands to a certain dimension, the code quality commences to deteriorate in some deep hashing models. For example, without NHL, the quality of hash codes in DSH experiences a marked decline when transitioning from 64 bits to 128 bits on the CIFAR-10 dataset. In contrast, with the incorporation of the NHL, this result undergoes a substantial improvement.

Besides, to analyze the influence of each component in the NHL, we conducted an ablation study on these models to investigate their impact. We devised several variants for the NHL, namely (i) NHL-basic: directly use E.q (2) to optimize the deep hashing model, (ii) NHL w/o D: without using

Table 2: The comparison of average mAP@K results with the original model is shown for NHL variants.

Data	NHL-basic	NHL w/o D	NHL w/o L	w/ NHL
CIFAR-10	+1.088%	+1.316%	+2.097%	+3.619%
ImageNet100	+2.209%	+2.823%	+2.434%	+4.364%
MSCOCO	+0.421%	+0.859%	+0.978%	+2.158%
avg.	+1.228%	+1.639%	+1.856%	+3.398%

the dominance-aware dynamic weighting strategy, (iii) NHL w/o L: without using the long-short cascade self-distillation. Table 2 presents the average performance changes across datasets for the models mentioned above. Overall, implementing NHL-basic, NHL w/o D, and NHL w/o L results in average performance improvements of 1.228%, 1.639%, and 1.856%, respectively. Employing only the dominance-aware dynamic weighting strategy (NHL w/o L) achieves the most significant relative improvement, highlighting the critical role of gradient optimization in this context. In Appendix F, we present the detailed results of various deep hashing models when utilizing the different variants of NHL.

4.3 Efficiency Analysis

In this experiment, we evaluated the deep hashing model's training time and memory usage. We recorded the total training time for the hashing model of five code lengths and recorded the maximal memory usage. Table 3 displays the results, where we selected CSQ and DCH as the deep hashing

Table 3: We evaluate efficiency on three datasets by recording the total training time for the deep hashing model with five code lengths and the maximum memory usage.

Data	Model	Tim	e (hours)	Memory	(GiB)
Data	Model	w/o NHL	w/ NHL	w/o NHL	w/ NHL
CIFAR-10	CSQ	0.455	$0.083 (5.48 \times)$	12.822	12.868
CIFAK-10	DCH	0.543	$0.085~(6.39\times)$	12.820	12.836
ImageNet100	CSQ	4.520	0.664 (6.81×)	12.923	13.139
magenerioo	DCH	6.025	1.161 (5.19×)	12.914	12.956
MSCOCO	CSQ	1.019	0.202 (5.05×)	12.906	13.067
MISCOCO	DCH	5.475	$0.981~(5.58\times)$	12.886	12.926

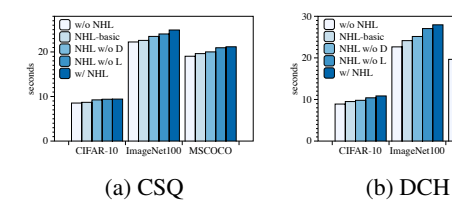


Figure 4: The average training time per epoch for CSQ and DCH across three datasets, using the traditional hash layer, NHL, or NHL variants.

models. These results demonstrate that the employment of the NHL incurs negligible additional memory expenses. This is attributed to the fact that during the training process, the primary memory usage stems from the parameters of the neural network, while the additional memory occupied by the target loss is relatively minimal. Meanwhile, the incorporation of the NHL can significantly enhance the overall training speed. It achieved an average training speedup of $5.94\times, 6\times$, and $5.31\times$ on the CIFAR-10, ImageNet-100, and MSCOCO datasets, respectively, across the two deep hashing models. In conjunction with the conclusions drawn from the previous experiment, this evidences that NHL can effectively expedite the training procedure without compromising the quality of hash codes.

Besides, we further analyze the average time per epoch during training across different NHL variants. Figure 4a and Figure 4b display the results of CSQ and DCH. Compared to deep hashing models without NHL (w/o NHL), incorporating NHL-basic, NHL w/o D, NHL w/o L, and w/ NHL led to a modest increase in training time of just 3.37%, 6.87%, 11.15%, and 13.75%, respectively.

4.4 Module Analysis

In this experiment, we conducted a comprehensive analysis of the Nested Hash Layer (NHL) from multiple perspectives, including (i) hyperparameter analysis and (ii) various code length settings. We utilize CSQ as the deep hashing model for the subsequent analysis. Additionally, we validated the performance of the Nested Hash Layer (NHL) under different backbone extractors, including other variants of ResNet and different architectures of Vision Transformers (ViT) [8]. For further details, please refer to Appendix E.2.

4.4.1 Parameter Sensitivity

In Eq.(9), λ serves as a hyperparameter that balances two objectives. We evaluated its values from $\{10^1, 10^0, 10^{-1}, 10^{-2}, 10^{-3}\}$ to calculate the mAP@K across three datasets. Figure 5 illustrates the results, highlighting that the performance of NHL demonstrates overall robustness to changes in λ . Generally, the optimal value is achieved when $\lambda=1$. Additionally, we conducted a parameter analysis on the learning rate, which is presented in Appendix E.1. The analysis indicates that the optimal range for the learning rate is $\{10^{-4}, 10^{-5}\}$.

4.4.2 More Code Length Settings

This section explores the results under a broader range of code length settings. We established three scenarios for code length: Case 1 sets a code length at every 32-bit interval, that is, $b = \{32 \times k\}_{k=1}^4$ and m = 4. Case 2 sets a code length at every 16-bit interval, that is, $b = \{16 \times k\}_{k=1}^8$ and m = 8. Case 3 sets a code length at every 8-bit interval, that is, $b = \{8 \times k\}_{k=1}^{16}$ and m = 16. Figure 6 presents the corresponding results. Here, the blue bars represent the average ratio of mAP@K at various lengths with and without using NHL. The yellow bars indicate the time cost ratio to complete training with and without using NHL. We observe that even with different code length settings, the use of NHL ensures a reduction in overall training time and improves the code quality. Moreover, it is noteworthy that the total training time does not monotonically increase with the number of output code lengths. For instance, the efficiency enhancement ratio in Case 3 is not as high as in Case 2. This is attributed to the requirement for the model to undergo more training iterations in Case 3 to ensure favorable outcomes across a greater number of code lengths.

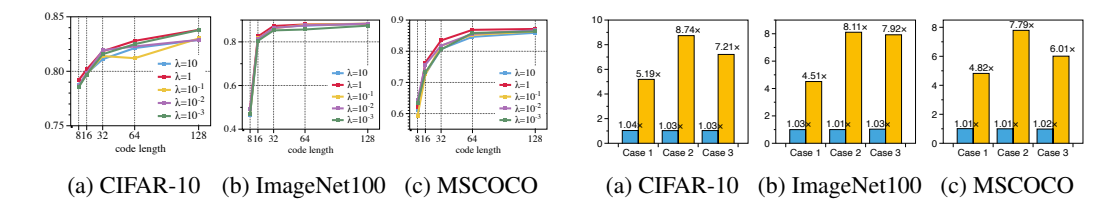


Figure 5: The mAP@K results across three datasets under varying λ values demonstrate that NHL is robust to λ to some extent.

Figure 6: Impact of NHL on average mAP@K ratio (blue bars) and training time cost ratio (yellow bars) across various code length settings.

Table 4: The mAP@K results across three datasets using different gradient conflict resolution strategies, with CSQ as the deep semantic hashing model. The best results are highlighted in bold, while the second-best results are underlined.

Mathad	Method CIFAR-10					ImageNet100						MSCOCO				
Method	8 bits	16 bits	32 bits	64 bits	128 bits	8 bits	16 bits	32 bits	64 bits	128 bits	8 bits	16 bits	32 bits	64 bits	128 bits	
NHL w/o D	0.707	0.773	0.815	0.823	0.831	0.451	0.803	0.846	0.873	0.884	0.638	0.769	0.822	0.866	0.877	
+ PCGrad	0.742	0.781	0.802	0.815	0.830	0.467	0.814	0.852	0.870	0.862	0.632	0.772	0.823	0.852	0.872	
+ GradDrop	0.739	0.764	0.805	0.802	0.828	0.461	0.815	0.859	0.872	0.861	0.636	0.776	0.827	0.861	0.875	
+ CAGrad	0.720	0.775	0.793	0.811	0.815	0.455	0.815	0.867	0.865	0.873	0.639	0.770	0.825	0.858	0.869	
+ RotoGrad	0.735	0.762	0.813	0.819	0.822	0.473	0.808	0.863	0.874	0.877	0.641	0.778	0.830	0.859	0.871	
NHL	0.792	0.802	0.818	0.828	0.838	0.495	0.825	0.873	0.880	0.882	0.659	0.778	0.847	0.878	0.881	
MAH	0.636	0.649	0.683	0.705	0.714	0.628	0.652	0.689	0.692	0.691	0.567	0.573	0.589	0.599	0.612	
SDMLH	0.617	0.684	0.723	0.748	0.763	0.526	0.557	0.618	0.623	0.644	0.602	0.646	0.737	0.761	0.814	

4.5 Compared with Gradient Conflicts Methods and Multi-length Hashing

In this section, we compare our proposed dominance-aware dynamic weighting strategy with other methods aimed at resolving gradient conflicts and two multi-length hashing. Specifically, we evaluate classic gradient conflicts approaches including PCGrad [44], GradDrop [6], CAGrad [26], and RotoGrad [15]. The comparison is conducted by replacing the dominance-aware dynamic weighting strategy in our NHL method with the gradient update strategies of these methods and then calculating the mAP@K results across three datasets, using CSQ as the deep hashing model. Besides, we also compared two multi-length hashing models MAH [30] and SDMLH [32]. Table 4 presents the results. It can be observed that, compared to other gradient conflict resolution approaches, our method achieves the best results in more cases. Furthermore, we notice that incorporating these methods often results in negative effects compared to not using any gradient conflict resolution strategy (NHL w/o D). We believe this is due to the nested structure of our parameters, which these classical methods fail to account for adequately. Additionally, the performance of the two multi-code length hashing models, MAH and SDMLH, under most scenarios lags behind that of the CSQ model combined with NHL. This underscores the importance of designing a plug-and-play module, as it allows seamless integration with more advanced deep hashing models to achieve superior retrieval results.

5 Conclusion

In this paper, we introduce the plug-and-play module NHL for deep hashing models. NHL allows these models to generate hash codes of different lengths simultaneously, simplifying training and reducing computational load. Additionally, the dominance-aware dynamic weighting strategy and long-short cascade self-distillation enhance NHL's effectiveness. We performed extensive experiments on three datasets to assess NHL's performance. The results show that NHL speeds up training while maintaining or improving retrieval effectiveness across various deep supervised hashing models. Our work mainly focuses on common symmetric deep supervised hashing methods, where both the database and query data use the same deep hashing network for generating hash codes. In contrast, NHL is limited to asymmetric deep supervised hashing methods [36, 16, 4, 41]. They use deep neural networks only for processing query, while direct or indirect optimization of hash codes in the database. Thus, simply changing the hash layer isn't enough for these methods. We believe that adding optimization designs for the database hash codes could be a promising solution.

References

- [1] Felix JS Bragman, Ryutaro Tanno, Sebastien Ourselin, Daniel C Alexander, and Jorge Cardoso. Stochastic filter groups for multi-task cnns: Learning specialist and generalist convolution kernels. In *Proceedings of the IEEE/CVF International Conference on Computer Vision*, pages 1385–1394, 2019.
- [2] Fatih Cakir, Kun He, Sarah Adel Bargal, and Stan Sclaroff. Hashing with mutual information. *IEEE transactions on pattern analysis and machine intelligence*, 41(10):2424–2437, 2019.
- [3] Yue Cao, Mingsheng Long, Bin Liu, and Jianmin Wang. Deep cauchy hashing for hamming space retrieval. In *Proceedings of the IEEE Conference on Computer Vision and Pattern Recognition*, pages 1229–1237, 2018.
- [4] Yudong Chen, Zhihui Lai, Yujuan Ding, Kaiyi Lin, and Wai Keung Wong. Deep supervised hashing with anchor graph. In *Proceedings of the IEEE/CVF international conference on computer vision*, pages 9796–9804, 2019.
- [5] Zhao Chen, Vijay Badrinarayanan, Chen-Yu Lee, and Andrew Rabinovich. Gradnorm: Gradient normalization for adaptive loss balancing in deep multitask networks. In *International conference on machine learning*, pages 794–803. PMLR, 2018.
- [6] Zhao Chen, Jiquan Ngiam, Yanping Huang, Thang Luong, Henrik Kretzschmar, Yuning Chai, and Dragomir Anguelov. Just pick a sign: Optimizing deep multitask models with gradient sign dropout. Advances in Neural Information Processing Systems, 33:2039–2050, 2020.
- [7] Jia Deng, Wei Dong, Richard Socher, Li-Jia Li, Kai Li, and Li Fei-Fei. Imagenet: A large-scale hierarchical image database. In *2009 IEEE conference on computer vision and pattern recognition*, pages 248–255. Ieee, 2009.
- [8] Alexey Dosovitskiy, Lucas Beyer, Alexander Kolesnikov, Dirk Weissenborn, Xiaohua Zhai, Thomas Unterthiner, Mostafa Dehghani, Matthias Minderer, Georg Heigold, Sylvain Gelly, et al. An image is worth 16x16 words: Transformers for image recognition at scale. In *International Conference on Learning Representations*, 2020.
- [9] Lixin Fan, Kam Woh Ng, Ce Ju, Tianyu Zhang, and Chee Seng Chan. Deep polarized network for supervised learning of accurate binary hashing codes. In *IJCAI*, pages 825–831, 2020.
- [10] Yuan Gao, Haoping Bai, Zequn Jie, Jiayi Ma, Kui Jia, and Wei Liu. Mtl-nas: Task-agnostic neural architecture search towards general-purpose multi-task learning. In *Proceedings of the IEEE/CVF Conference on computer vision and pattern recognition*, pages 11543–11552, 2020.
- [11] SHI Guangyuan, Qimai Li, Wenlong Zhang, Jiaxin Chen, and Xiao-Ming Wu. Recon: Reducing conflicting gradients from the root for multi-task learning. In *The Eleventh International Conference on Learning Representations*, 2022.
- [12] Michelle Guo, Albert Haque, De-An Huang, Serena Yeung, and Li Fei-Fei. Dynamic task prioritization for multitask learning. In *Proceedings of the European conference on computer vision (ECCV)*, pages 270–287, 2018.
- [13] Kaiming He, Xiangyu Zhang, Shaoqing Ren, and Jian Sun. Deep residual learning for image recognition. In *Proceedings of the IEEE conference on computer vision and pattern recognition*, pages 770–778, 2016.
- [14] Jiun Tian Hoe, Kam Woh Ng, Tianyu Zhang, Chee Seng Chan, Yi-Zhe Song, and Tao Xiang. One loss for all: Deep hashing with a single cosine similarity based learning objective. *Advances in Neural Information Processing Systems*, 34:24286–24298, 2021.
- [15] Adrian Javaloy and Isabel Valera. Rotograd: Gradient homogenization in multitask learning. In *The Tenth International Conference on Learning Representations (Virtual)*, 2022.
- [16] Qing-Yuan Jiang and Wu-Jun Li. Asymmetric deep supervised hashing. In *Proceedings of the AAAI conference on artificial intelligence*, volume 32, 2018.

- [17] Alex Kendall, Yarin Gal, and Roberto Cipolla. Multi-task learning using uncertainty to weigh losses for scene geometry and semantics. In *Proceedings of the IEEE conference on computer vision and pattern recognition*, pages 7482–7491, 2018.
- [18] Diederik P Kingma and Jimmy Ba. Adam: A method for stochastic optimization. *arXiv preprint arXiv:1412.6980*, 2014.
- [19] Iasonas Kokkinos. Ubernet: Training a universal convolutional neural network for low-, mid-, and high-level vision using diverse datasets and limited memory. In *Proceedings of the IEEE conference on computer vision and pattern recognition*, pages 6129–6138, 2017.
- [20] Alex Krizhevsky, Geoffrey Hinton, et al. Learning multiple layers of features from tiny images. 2009.
- [21] Aditya Kusupati, Gantavya Bhatt, Aniket Rege, Matthew Wallingford, Aditya Sinha, Vivek Ramanujan, William Howard-Snyder, Kaifeng Chen, Sham Kakade, Prateek Jain, et al. Matryoshka representation learning. *Advances in Neural Information Processing Systems*, 35:30233–30249, 2022.
- [22] Taeho Lee and Junhee Seok. Multi task learning: A survey and future directions. In 2023 International Conference on Artificial Intelligence in Information and Communication (ICAIIC), pages 232–235. IEEE, 2023.
- [23] Y Li, W Pei, Yufei Zha, and JC van Gemert. Push for quantization: Deep fisher hashing. In 30th British Machine Vision Conference, BMVC 2019, 2020.
- [24] Tsung-Yi Lin, Michael Maire, Serge Belongie, James Hays, Pietro Perona, Deva Ramanan, Piotr Dollár, and C Lawrence Zitnick. Microsoft coco: Common objects in context. In *Computer Vision–ECCV 2014: 13th European Conference, Zurich, Switzerland, September 6-12, 2014, Proceedings, Part V 13*, pages 740–755. Springer, 2014.
- [25] Bin Liu, Yue Cao, Mingsheng Long, Jianmin Wang, and Jingdong Wang. Deep triplet quantization. In *Proceedings of the 26th ACM international conference on Multimedia*, pages 755–763, 2018.
- [26] Bo Liu, Xingchao Liu, Xiaojie Jin, Peter Stone, and Qiang Liu. Conflict-averse gradient descent for multi-task learning. Advances in Neural Information Processing Systems, 34:18878–18890, 2021.
- [27] Haomiao Liu, Ruiping Wang, Shiguang Shan, and Xilin Chen. Deep supervised hashing for fast image retrieval. In *Proceedings of the IEEE conference on computer vision and pattern recognition*, pages 2064–2072, 2016.
- [28] Shikun Liu, Edward Johns, and Andrew J Davison. End-to-end multi-task learning with attention. In *Proceedings of the IEEE/CVF conference on computer vision and pattern recognition*, pages 1871–1880, 2019.
- [29] Xiao Luo, Haixin Wang, Daqing Wu, Chong Chen, Minghua Deng, Jianqiang Huang, and Xian-Sheng Hua. A survey on deep hashing methods. ACM Transactions on Knowledge Discovery from Data, 17(1):1–50, 2023.
- [30] Yadan Luo, Zi Huang, Yang Li, Fumin Shen, Yang Yang, and Peng Cui. Collaborative learning for extremely low bit asymmetric hashing. *IEEE Transactions on Knowledge and Data Engineering*, 33(12):3675–3685, 2020.
- [31] Devraj Mandal, Yashas Annadani, and Soma Biswas. Growbit: Incremental hashing for cross-modal retrieval. In *Computer Vision–ACCV 2018: 14th Asian Conference on Computer Vision, Perth, Australia, December 2–6, 2018, Revised Selected Papers, Part IV 14*, pages 305–321. Springer, 2019.
- [32] Xiushan Nie, Xingbo Liu, Jie Guo, Letian Wang, and Yilong Yin. Supervised discrete multiple-length hashing for image retrieval. *IEEE Transactions on Big Data*, 9(1):312–327, 2022.

- [33] Zexuan Qiu, Qinliang Su, Zijing Ou, Jianxing Yu, and Changyou Chen. Unsupervised hashing with contrastive information bottleneck. In *Proceedings of the Thirtieth International Joint Conference on Artificial Intelligence, IJCAI 2021, Virtual Event / Montreal, Canada, 19-27 August 2021*, pages 959–965, 2021.
- [34] Sebastian Ruder, Joachim Bingel, Isabelle Augenstein, and Anders Søgaard. Latent multitask architecture learning. In *Proceedings of the AAAI conference on artificial intelligence*, volume 33, pages 4822–4829, 2019.
- [35] Mark Sandler, Andrew Howard, Menglong Zhu, Andrey Zhmoginov, and Liang-Chieh Chen. Mobilenetv2: Inverted residuals and linear bottlenecks. In *Proceedings of the IEEE conference on computer vision and pattern recognition*, pages 4510–4520, 2018.
- [36] Fumin Shen, Xin Gao, Li Liu, Yang Yang, and Heng Tao Shen. Deep asymmetric pairwise hashing. In *Proceedings of the 25th ACM international conference on Multimedia*, pages 1522–1530, 2017.
- [37] Yuan Sun, Dezhong Peng, Jian Dai, and Zhenwen Ren. Stepwise refinement short hashing for image retrieval. In *Proceedings of the 31st ACM International Conference on Multimedia*, pages 6501–6509, 2023.
- [38] Liangdao Wang, Yan Pan, Hanjiang Lai, and Jian Yin. Image retrieval with well-separated semantic hash centers. In *Proceedings of the Asian Conference on Computer Vision*, pages 978–994, 2022.
- [39] Liangdao Wang, Yan Pan, Cong Liu, Hanjiang Lai, Jian Yin, and Ye Liu. Deep hashing with minimal-distance-separated hash centers. In *Proceedings of the IEEE/CVF Conference on Computer Vision and Pattern Recognition*, pages 23455–23464, 2023.
- [40] Xiaofang Wang, Yi Shi, and Kris M Kitani. Deep supervised hashing with triplet labels. In *Computer Vision–ACCV 2016: 13th Asian Conference on Computer Vision, Taipei, Taiwan, November 20-24, 2016, Revised Selected Papers, Part I 13*, pages 70–84. Springer, 2017.
- [41] Dayan Wu, Qi Dai, Bo Li, and Weiping Wang. Deep uncoupled discrete hashing via similarity matrix decomposition. *ACM Transactions on Multimedia Computing, Communications and Applications*, 19(1):1–22, 2023.
- [42] Dayan Wu, Qinghang Su, Bo Li, and Weiping Wang. Efficient hash code expansion by recycling old bits. In *Proceedings of the 30th ACM International Conference on Multimedia*, pages 572–580, 2022.
- [43] Dayan Wu, Qinghang Su, Bo Li, and Weiping Wang. Pairwise-label-based deep incremental hashing with simultaneous code expansion. In *Proceedings of the AAAI Conference on Artificial Intelligence*, volume 38, pages 9169–9177, 2024.
- [44] Tianhe Yu, Saurabh Kumar, Abhishek Gupta, Sergey Levine, Karol Hausman, and Chelsea Finn. Gradient surgery for multi-task learning. *Advances in Neural Information Processing Systems*, 33:5824–5836, 2020.
- [45] Li Yuan, Tao Wang, Xiaopeng Zhang, Francis EH Tay, Zequn Jie, Wei Liu, and Jiashi Feng. Central similarity quantization for efficient image and video retrieval. In *Proceedings of the IEEE/CVF conference on computer vision and pattern recognition*, pages 3083–3092, 2020.
- [46] Shu Zhao, Dayan Wu, Wanqian Zhang, Yu Zhou, Bo Li, and Weiping Wang. Asymmetric deep hashing for efficient hash code compression. In *Proceedings of the 28th ACM International Conference on Multimedia*, pages 763–771, 2020.
- [47] Xiangtao Zheng, Yichao Zhang, and Xiaoqiang Lu. Deep balanced discrete hashing for image retrieval. *Neurocomputing*, 403:224–236, 2020.
- [48] Han Zhu, Mingsheng Long, Jianmin Wang, and Yue Cao. Deep hashing network for efficient similarity retrieval. In *Proceedings of the AAAI conference on Artificial Intelligence*, volume 30, 2016.
- [49] Hao Zhu, Shenghua Gao, et al. Locality constrained deep supervised hashing for image retrieval. In *IJCAI*, pages 3567–3573, 2017.

Appendix

A Experimental Settings

A.1 Datasets

We conducted experiments on three widely used datasets in deep hashing for evaluation. **CIFAR-10** [20] consists of 60,000 images from 10 classes. Following [3], we randomly select 1,000 images per class as the query set, and 500 images per class as the training set, and use all remaining images as the database. **ImageNet100** is a subset of ImageNet [7] with 100 classes. We follow the settings from [9] and randomly select 100 categories. Then, we use all the images of these categories in the training set as the database and the images in the validation set as the queries. Furthermore, we randomly select 13,000 as the training images from the database. **MSCOCO** [24] is a large-scale multi-label dataset. We consider a subset of 122,218 images from 80 categories, as in previous works [33]. We randomly select 5,000 images from the subset as the query set and use the remaining images as the database. For training, we randomly select 10,000 images from the database. As in most deep hashing settings, two samples are viewed as similar if they correspond to the same label on CIFAR-10 and ImageNet100. For multi-label datasets MSCOCO, two samples are considered similar if they share at least one common label.

A.2 Baselines and Evaluation Metric

We considered the following deep supervised hashing models: DSH [27], DHN [48], DTSH [40], LCDSH [49], DCH [3], DBDH [47], CSQ [45], SHCIR [38], DPN [9], and MDSH [39]. For all the above models, we uniformly adopted ResNet50 [13] as the backbone to extract 2048-dimensional image features.

We employed the mean Average Precision at the top K (mAP@K) as the evaluation metric. Specifically, we utilized mAP@ALL for CIFAR-10, mAP@5000 for MSCOCO, and mAP@1000 for ImageNet100, following the settings used in previous studies [33, 9]. Unless otherwise specified, we set the hash code lengths $b \in \{8, 16, 32, 64, 128\}$ for the following experiments, as these lengths are prevalently used in previous works.

A.3 Training Details

For the deep hashing models we adopted, we endeavored to implement all models using PyTorch, based on the code repositories provided in the original papers and the implementation details described therein. The experiments were conducted on a Linux server equipped with 8 NVIDIA GeForce RTX 4090 GPUs. For each model (including those integrated with NHL), a single NVIDIA GeForce RTX 4090 GPU was utilized for both training and testing. Among these models, DHN and DBDH failed to produce valid results on ImageNet100 due to the absence of hyperparameter settings in the original papers, and our grid search method was unable to identify suitable parameters. Additionally, the SHCIR and MDSH models did not propose methods for handling multi-label datasets (e.g., MSCOCO) in their original publications. The batch size B was set to 64. When applying NHL to the deep hashing models, we employed the Adam optimizer [18] and selected the learning rate from $\{10^{-4}, 10^{-5}\}$. The hyperparameter λ was set to 1. A grid search method was conducted across different scenarios to identify the optimal combination.

B Proofs

Proposition 1. Assume $\theta_{ij}^{(k)}$ is the angle between two gradients $g_i^{(k)}$ and $g_j^{(k)}$, and $\|\cdot\|$ denotes the Frobenius norm, if the following inequality holds:

$$\alpha_k \|g_k^{(k)}\| + \sum_{k < i < m} \alpha_i cos\theta_{ik}^{(k)} \|g_i^{(k)}\| \ge 0, \tag{10}$$

then the update of $W^{(k)}$ is guaranteed to be align-domination.

Proof. Align-domination is satisfied if the inner product between the total gradient $g^{(k)} = \sum_{i=k}^{m} \alpha_i g_i^{(k)}$ and the dominant gradient $g_k^{(k)}$ is non-negative:

$$\langle g^{(k)}, g_k^{(k)} \rangle \ge 0.$$

Expanding the inner product:

$$\langle g^{(k)}, g_k^{(k)} \rangle = \alpha_k \|g_k^{(k)}\|^2 + \sum_{k < i < m} \alpha_i \|g_i^{(k)}\| \|g_k^{(k)}\| \cos \theta_{ik}^{(k)}.$$

Dividing through by $\|g_k^{(k)}\|$ (assuming $\|g_k^{(k)}\| > 0$), we obtain:

$$\alpha_k \|g_k^{(k)}\| + \sum_{k < i \le m} \alpha_i \cos \theta_{ik}^{(k)} \|g_i^{(k)}\| \ge 0.$$

Thus, if the inequality holds, the inner product $\langle g^{(k)}, g_k^{(k)} \rangle \geq 0$, ensuring that the total gradient $g^{(k)}$ is aligned with the dominant gradient $g_k^{(k)}$. This confirms align-domination for the update of $\mathcal{W}^{(k)}$.

Proposition 2. If the following inequality holds for all $k < i \le m$, then Eq. (10) also holds.

$$\alpha_i cos\theta_{ik}^{(k)} \|g_i^{(k)}\| + \frac{\alpha_k}{m-k} \|g_k^{(k)}\| \ge 0.$$
 (11)

Proof. For any fixed k and $k < i \le m$, Eq. (11) can be rewritten as:

$$\alpha_i \cos \theta_{ik}^{(k)} \|g_i^{(k)}\| \ge -\frac{\alpha_k}{m-k} \|g_k^{(k)}\|. \tag{12}$$

This inequality establishes a lower bound on the contribution of each term $\alpha_i \cos \theta_{ik}^{(k)} ||g_i^{(k)}||$ for $k < i \le m$. Then, summing Eq. (12) over all $k < i \le m$, we obtain:

$$\sum_{k < i \le m} \alpha_i \cos \theta_{ik}^{(k)} \|g_i^{(k)}\| \ge \sum_{k < i \le m} -\frac{\alpha_k}{m-k} \|g_k^{(k)}\|.$$
(13)

Since there are exactly m-k terms in the summation over $k < i \le m$, the right-hand side simplifies to:

$$\sum_{k < i \le m} -\frac{\alpha_k}{m-k} \|g_k^{(k)}\| = -(m-k) \cdot \frac{\alpha_k}{m-k} \|g_k^{(k)}\| = -\alpha_k \|g_k^{(k)}\|.$$
 (14)

Thus, we have:

$$\alpha_k \|g_k^{(k)}\| + \sum_{k < i \le m} \alpha_i \cos \theta_{ik}^{(k)} \|g_i^{(k)}\| \ge 0.$$
 (15)

This proves that Eq. (10) holds whenever Eq. (11) holds for all $k < i \le m$.

C The Method to Solve Linear Programming Problem Eq. 5

In the dominance-aware dynamic weighting strategy, we propose the following target for the objective weights $\{\alpha_k\}_{k=1}^m$:

$$\alpha_i \cos \theta_{ik}^{(k)} \|g_i^{(k)}\| + \frac{\alpha_k}{m-k} \|g_k^{(k)}\| \ge 0; \ k \le i \le m.$$
 (16)

This section describes how to solve it. Without loss of generality, we first set $\alpha_1=1$ for the shortest code' objective \mathcal{L}_1 , as normalization can subsequently be applied. Then we introduce $\alpha_i^{(k)}$ denote only consider to ensure that L_i and L_k satisfy Eq. (16) on $\mathcal{W}^{(k)}$. Using $cos\theta_{ik}^{(k)} = \frac{g_i^{(k)}g_k^{(k)}}{\|g_i^{(k)}\|\|g_k^{(k)}\|}$ and re-arranging terms, we then get:

$$\alpha_i^{(k)}(-g_i^{(k)}g_k^{(k)}) \le \frac{\alpha_k}{m-k} \|g_k^{(k)}\|^2; \ k \le i \le m.$$
(17)

Algorithm 1 The training algorithm with NHL

```
Input: training samples X = \{x_1, x_2, ... x_N\}, the hyper-parameters \lambda.
 1: Initialization: the parameter of the deep hashing model \{\theta_F, \mathcal{W}\}, \alpha_k = 1 for \forall k.
 2: repeat
         draw a mini-batch \{x_1, x_2, ..., x_B\} from X to compute \{\mathcal{L}_k\}_{k=1}^m using standard forward
         propagation algorithm
         for each k \in \{1, 2, ...., m\} do
 4:
            for each i \in \{1, 2, ...., m\} do
 5:
                obtain g_i^{(k)} by computing standard gradients g_i^{(k)}=\frac{\partial \mathcal{L}_i}{\partial \mathcal{W}^{(k)}} {Only calculating the gradients
 6:
                ents on \{\mathcal{W}^{(k)}\}_{k=1}^m\}
            end for
 7:
 8:
         end for
        compute \{\alpha_k\}_{k=1}^m by Eq. (7) and Eq. (6) renormalize \{\alpha_k\}_{k=1}^m so that \sum_{k=1}^m \alpha_k = m update parameters of the deep hashing model by minimizing Eq. (9) using the standard
 9:
10:
         backpropagation algorithm
12:
         if achieved a smaller \mathcal{L}_k then
             record the current model parameters \theta_E^{(k)}, \mathcal{W}^{(k)} for the model of length b_k.
13:
15: until converged
Output: parameters of deep hashing model \{\theta_F^{(k)}\}_{k=1}^m and \{\mathcal{W}^{(k)}\}_{k=1}^m
```

If $g_i^{(k)}g_k^{(k)} \geq 0$, because $\alpha_j > 0$ for j=1,2,...,m, the inequality invariably holds. Then we set $\alpha_i^{(k)} = 1$. If the case that $g_i^{(k)}g_k^{(k)} < 0$, we can get:

$$\alpha_i^{(k)} \le \frac{\alpha_k}{k - m} \frac{\|g_k^{(k)}\|^2}{g_i^{(k)} g_k^{(k)}}; \ k \le i \le m.$$
(18)

Since our target is to minimize the impact on other optimization objectives while avoiding antidomination as much as possible, we equate the terms on both sides of Eq.18, ultimately deriving the solution:

$$\alpha_i^{(k)} = \begin{cases} 1 & \text{if } g_i^{(k)} \cdot g_k^{(k)} \ge 0\\ \frac{\alpha_k}{k - m} \frac{\|g_k^{(k)}\|^2}{g_i^{(k)} g_k^{(k)}} & \text{if } g_i^{(k)} \cdot g_k^{(k)} < 0; k \le i \le m \end{cases}$$

$$(19)$$

Then, consider \mathcal{L}_i and all \mathcal{L}_k , k < i, the α_i is as follows:

$$\alpha_i = \min(\alpha_i^{(1)}, \alpha_i^{(2)}, ..., \alpha_i^{(i)}). \tag{20}$$

It is evident that the computational complexity of calculating $\alpha_i^{(k)}$ is $O(lb_k)$, where l represents the dimension of the data feature v. Consequently, the overall computational complexity amounts to $O(lb_m m^2)$, where the b_m is the longest code length.

D The Training Algorithm

In this section, we first present the training algorithm of our proposed NHL in Algorithm 1. Then, we elaborate on the details of our training process. As we discussed in Section 3.5, throughout the training procedure, we monitor the value of each L_k and save the model parameters when each L_k reaches its minimum to output the corresponding hash codes $h^{(k)}$. In lines 12-14 of Algorithm 1, when a smaller L_k is achieved, We record the current model parameters θ_F and $\mathcal W$ as the parameters of the model with a length of b_k , denoted as $\theta_F^{(k)}$ and $\mathcal W^{(k)}$.

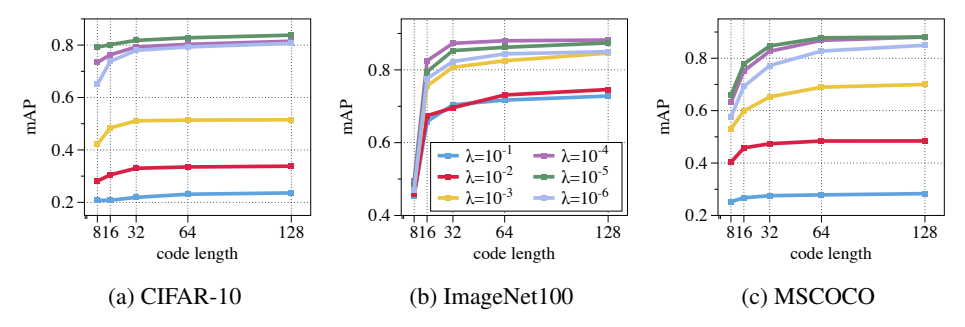


Figure 7: The mAP@K results across three datasets under different learning rates.

Table 5: The mAP@K evaluation when using different feature extraction networks as the backbone of CSQ across three datasets. We compared the results of using NHL (w/ NHL) with those of not using NHL (w/o NHL) on these three datasets.

Data	Backbone		w/o N	HL (The	Original 1	Model)					w/ NHL		
Data	Баскоопе	8 bits	16 bits	32 bits	64 bits	128 bits	avg.	8 bits	16 bits	32 bits	64 bits	128 bits	avg.
	ResNet18	0.654	0.710	0.743	0.717	0.739	0.712	0.664	0.718	0.762	0.793	0.817	0.750 (+5.36%)
CIFAR-10	ResNet34	0.682	0.700	0.724	0.730	0.722	0.711	0.691	0.724	0.757	0.787	0.826	0.757 (+6.37%)
(mAP@ALL)	ResNet50	0.762	0.786	0.798	0.798	0.807	0.790	0.792	0.802	0.818	0.828	0.838	0.816 (+3.21%)
	MobileNetV2	0.661	0.725	0.750	0.774	0.788	0.739	0.677	0.735	0.779	0.799	0.816	0.761 (+2.92%)
	ViT_B_16	0.891	0.903	0.907	0.912	0.913	0.905	0.895	0.909	0.919	0.931	0.937	0.918 (+1.44%)
ImageNet100	ResNet18	0.375	0.727	0.754	0.773	0.795	0.684	0.413	0.722	0.774	0.804	0.815	0.705 (+3.03%)
	ResNet34	0.398	0.773	0.815	0.836	0.839	0.732	0.465	0.784	0.828	0.850	0.855	0.756 (+3.31%)
(mAP@1000)	ResNet50	0.456	0.822	0.860	0.877	0.878	0.778	0.495	0.825	0.873	0.880	0.882	0.787 (+1.59%)
(IIIAF @ 1000)	MobileNetV2	0.414	0.679	0.745	0.788	0.802	0.685	0.422	0.708	0.759	0.800	0.819	0.701 (+2.33%)
	ViT_B_16	0.523	0.888	0.910	0.915	0.915	0.830	0.533	0.887	0.906	0.918	0.925	0.834 (+0.43%)
	ResNet18	0.532	0.653	0.745	0.792	0.811	0.706	0.576	0.679	0.760	0.807	0.824	0.729 (+3.19%)
MSCOCO	ResNet34	0.554	0.715	0.789	0.830	0.836	0.744	0.591	0.731	0.802	0.840	0.847	0.762 (+2.33%)
(mAP@5000)	ResNet50	0.596	0.750	0.847	0.877	0.871	0.788	0.659	0.778	0.847	0.878	0.881	0.809 (+2.58%)
	MobileNetV2	0.543	0.668	0.742	0.806	0.823	0.716	0.578	0.691	0.766	0.815	0.836	0.737 (+2.90%)
	ViT_B_16	0.638	0.790	0.883	0.895	0.906	0.822	0.675	0.794	0.889	0.898	0.902	0.831 (+1.12%)

E More Experimental Analyses

E.1 Hyper-parameters

We further conducted experimental validation on the CSQ model under different learning rate settings. We set the learning rates to $\{10^{-1}, 10^{-2}, 10^{-3}, 10^{-4}, 10^{-5}, 10^{-6}\}$ and performed experiments across three datasets. Figure 7 presents the results. Based on this experiment, we determined the optimal learning rate range to be $\{10^{-4}, 10^{-5}\}$.

E.2 Backbone Analysis

The NHL is designed for versatile integration with various deep supervised hashing models. To rigorously validate the generalizability of NHL, we extended this investigation by incorporating it into the CSQ deep hashing model while utilizing a diverse range of alternative backbone architectures for feature extraction. Specifically, we experimented with ResNet variants of different scales, including ResNet18 and ResNet34. We also present the results of ResNet50 used previously for comparison. Furthermore, to assess NHL's compatibility with distinct network structures, we also employed the Vision Transformer (ViT_B_16) [8] and the lightweight MobileNetV2 architecture [35]. As demonstrated in Table 5, NHL consistently maintains its effectiveness when paired with these varied backbones. This underscores NHL's broad applicability and its robustness in enhancing hashing performance across different types and scales of feature extractors, from various CNNs to transformer-based models.

F Ablation Study

This section presents the comprehensive results of NHL variants applied to deep hashing models. Figures 8, 6, and 7 showcase the outcomes for CIFAR-10, ImageNet100, and MSCOCO, respectively. The best results are highlighted in bold, while the second-best results are underlined. From these results, it is evident that in the vast majority of cases, employing the complete NHL method achieves

optimal performance. Additionally, in certain scenarios, using variants of NHL yields the best results, which can be attributed to the inherent differences among various deep hashing models, as well as the influence of different hash code lengths and datasets. As a plug-and-play module, NHL demonstrates sufficient robustness and adaptability across diverse applications.

Table 6: The mAP@K comparison results on the ImageNet100 dataset when different deep hashing models use the original hash layer, NHL, or the variants of NHL. The best results are highlighted in bold, while the second-best results are underlined.

Data	Length	NHL	DSH	DTSH	LCDSH	DCH	CSQ	DPN	SHCIR	MDSH
		w/o	0.703	0.432	0.248	0.776	0.456	0.436	0.789	0.785
		-basic	0.630	0.544	0.407	0.809	0.424	0.453	0.744	0.697
	8bit	w/o D	0.688	0.512	0.413	0.810	0.451	0.456	0.764	0.787
		w/o L	0.663	0.535	0.426	0.797	0.487	0.453	0.777	0.756
		w/	0.755	0.552	0.422	0.809	0.495	0.487	0.798	0.794
		w/o	0.808	0.710	0.395	0.834	0.822	0.827	0.861	0.845
		-basic	0.787	0.682	0.571	0.845	0.781	0.830	0.831	0.812
	16bit	w/o D	0.797	0.701	0.597	0.846	0.803	0.832	0.822	0.836
		w/o L	0.784	0.721	0.554	0.839	0.820	0.825	0.828	0.827
		w/	0.816	0.714	0.568	0.842	0.825	0.829	0.881	0.851
		w/o	0.827	0.770	0.542	0.845	0.860	0.864	0.879	0.874
ImageNet100		-basic	0.814	0.765	0.622	0.856	0.847	0.862	0.867	0.859
(mAP@1000)	32bit	w/o D	0.808	0.721	0.645	0.858	0.846	0.861	0.867	0.846
(IIIAF @ 1000)		w/o L	0.807	0.749	0.601	0.850	0.848	0.858	0.861	0.860
		w/	0.829	0.766	0.628	0.855	0.873	0.860	0.889	0.878
		w/o	0.828	0.784	0.608	0.859	0.877	0.870	0.883	0.895
		-basic	0.825	0.773	0.671	0.864	0.874	0.875	0.881	0.879
	64bit	w/o D	0.818	0.760	0.679	0.863	0.873	0.874	0.885	0.872
		w/o L	0.820	0.769	0.631	0.854	0.864	0.870	0.882	0.879
		w/	0.838	0.788	0.657	0.860	0.880	0.877	0.893	0.884
		w/o	0.822	0.803	0.692	0.848	0.878	0.877	0.881	0.894
		-basic	0.827	0.782	0.703	0.863	0.888	0.878	0.887	0.888
	128bit	w/o D	0.820	0.764	0.714	0.866	0.884	0.880	0.884	0.883
		w/o L	0.825	0.770	0.665	0.857	0.878	0.877	0.887	0.886
		w/	0.841	0.792	0.692	<u>0.863</u>	0.882	0.881	0.898	0.896

Table 7: The mAP@K comparison results on the MSCOCO dataset when different deep hashing models use the original hash layer, NHL, or the variants of NHL. The best results are highlighted in bold, while the second-best results are underlined.

Data	Length	NHL	DSH	DHN	DTSH	LCDSH	DCH	DBDH	CSQ	DPN
		w/o	0.685	0.659	0.706	0.687	0.695	0.655	0.596	0.575
		-basic	0.693	0.714	0.737	0.708	0.720	0.676	0.635	0.621
	8bit	w/o D	0.662	0.705	0.738	0.727	0.721	0.690	0.638	0.633
		w/o L	0.688	0.708	0.734	0.703	0.692	0.688	0.636	0.646
		w/	0.714	0.724	0.751	0.713	0.723	0.692	0.659	0.638
		w/o	0.722	0.751	0.770	0.769	0.756	0.727	0.750	0.757
		-basic	<u>0.730</u>	0.757	0.769	0.757	0.768	0.732	0.735	0.747
	16bit	w/o D	0.705	0.751	0.775	<u>0.771</u>	0.773	0.737	<u>0.769</u>	0.779
		w/o L	0.726	0.764	0.789	0.761	0.736	0.747	0.749	0.774
		w/	0.735	0.760	0.793	0.773	0.769	0.748	0.778	0.769
		w/o	0.757	0.786	0.810	0.787	0.762	0.760	0.847	0.828
MSCOCO		-basic	0.747	0.789	0.791	0.774	0.788	0.764	0.822	0.820
(mAP@1000)	32bit	w/o D	0.731	0.783	0.805	0.788	0.787	0.765	0.822	0.835
(111741 @ 1000)		w/o L	0.749	0.792	0.809	0.789	0.757	0.781	0.811	0.819
		w/	0.764	0.794	0.819	0.794	0.786	0.778	0.847	0.837
		w/o	0.779	0.810	0.823	0.825	0.777	0.769	0.877	0.862
		-basic	0.765	0.809	0.796	0.780	0.791	0.783	0.866	0.853
	64bit	w/o D	0.749	0.804	0.808	0.798	<u>0.789</u>	0.783	0.866	0.860
		w/o L	0.765	0.815	0.814	<u>0.826</u>	0.765	0.803	0.857	0.849
		w/	0.789	0.837	0.823	0.828	<u>0.789</u>	0.809	0.881	0.872
		w/o	0.769	0.832	0.831	<u>0.836</u>	0.734	0.800	0.871	0.863
		-basic	0.773	0.820	0.797	0.786	0.787	0.799	0.876	0.868
	128bit	w/o D	0.761	0.822	0.814	0.802	0.787	0.797	0.877	0.872
		w/o L	0.774	0.828	0.815	0.839	0.764	0.811	0.873	0.866
		w/	0.789	0.837	0.823	0.828	0.789	0.809	0.881	0.872

Table 8: The mAP@K comparison results on the CIFAR-10 dataset when different deep hashing models use the original hash layer, NHL, or the variants of NHL. The best results are highlighted in bold, while the second-best results are underlined.

Data	Length	NHL	DSH	DHN	DTSH	LCDSH	DCH	DBDH	CSQ	DPN	SHCIR	MDSH
		w/o	0.690	0.718	0.754	0.715	0.776	0.737	0.762	0.703	0.754	0.755
		-basic	0.598	0.724	0.560	0.759	0.779	0.731	0.652	0.731	0.761	0.752
	8bit	w/o D	0.620	0.730	0.772	0.751	0.772	0.750	0.707	0.727	0.740	0.743
		w/o L	0.641	0.752	0.747	0.773	0.781	0.737	0.769	0.632	0.760	0.760
		w/	0.717	0.739	0.766	0.775	0.787	0.748	0.792	0.729	0.758	0.762
		w/o	0.731	0.765	0.778	0.771	0.802	0.771	0.786	0.757	0.791	0.808
		-basic	0.688	0.778	0.702	0.782	0.806	0.769	0.758	0.768	0.796	0.788
	16bit	w/o D	0.667	0.769	0.785	0.766	0.798	0.770	0.773	0.783	0.777	0.775
		w/o L	0.710	0.797	0.775	0.785	0.808	0.764	0.777	0.752	0.793	0.801
		w/	0.732	0.776	0.790	0.799	0.810	0.785	0.802	0.765	0.797	0.811
		w/o	0.740	0.813	0.799	0.817	0.829	0.796	0.798	0.790	0.820	0.829
CIFAR-10		-basic	0.726	0.818	0.777	0.815	0.827	0.797	0.795	0.804	0.834	0.823
(mAP@1000)	32bit	w/o D	0.733	0.783	0.814	0.788	0.822	0.799	0.815	0.812	0.812	0.814
(IIIAF @ 1000)		w/o L	0.739	0.815	0.796	0.799	0.828	0.793	0.803	0.792	0.828	0.831
		w/	0.744	0.824	0.802	0.825	0.833	0.804	0.818	0.795	0.824	0.838
		w/o	0.727	0.837	0.831	0.826	0.830	0.829	0.798	0.804	0.844	0.844
		-basic	0.734	0.834	0.810	0.823	0.834	0.822	0.812	0.819	0.853	0.845
	64bit	w/o D	0.740	0.802	0.820	0.803	0.827	0.811	0.823	0.817	0.834	0.838
		w/o L	0.739	0.833	0.808	0.814	0.835	0.816	0.821	0.819	0.848	0.849
		w/	0.743	0.835	0.822	0.839	0.843	0.825	0.828	0.826	0.849	0.852
		w/o	0.381	0.853	0.811	0.854	0.825	0.829	0.807	0.819	0.828	0.832
		-basic	0.752	0.846	0.835	0.835	0.829	0.838	0.824	0.824	0.827	0.852
	128bit	w/o D	0.744	0.821	0.831	0.824	0.831	0.834	0.831	0.821	0.838	0.845
		w/o L	0.736	0.852	0.818	0.828	0.839	0.873	0.832	0.827	0.857	0.858
		w/	0.749	0.866	0.836	0.868	0.844	0.844	0.838	0.824	0.848	0.861